Science of the Total Environment 914 (2024) 169932

Contents lists available at ScienceDirect

Science of the Total Environment

journal homepage: www.elsevier.com/locate/scitotenv

Influence of phosphate on bacterial release from activated carbon point-of-use filters and on biofilm characteristics

Gemma G. Clark [a,*], Dietrich Geisler [b], Evan J. Coey [a], Lance J. Pollitz [a], Farzana R. Zaki [c], Conghui Huang [a], Stephen A. Boppart [c,d,e], Thanh H. Nguyen [a,e,f]

[a] Department of Civil and Environmental Engineering, University of Illinois at Urbana-Champaign, United States of America
[b] Department of Computer Science, Cornell University, United States of America
[c] Beckman Institute for Advanced Science and Technology, University of Illinois at Urbana-Champaign, United States of America
[d] Department of Bioengineering, Department of Electrical and Computer Engineering, University of Illinois at Urbana-Champaign, United States of America
[e] Carle Illinois College of Medicine, United States of America
[f] Institute of Genomic Biology, University of Illinois at Urbana-Champaign, United States of America

HIGHLIGHTS

- Phosphate filters released fewer bacteria than groundwater filters.
- Phosphate biofilms were thicker and rougher than groundwater biofilms.
- Overall porosity did not differ between groundwater and phosphate biofilms.
- Phosphate biofilms had fewer pores per volume of biofilm than groundwater biofilms.
- Phosphate biofilms had shorter pore-connecting channels than groundwater biofilms.

GRAPHICAL ABSTRACT

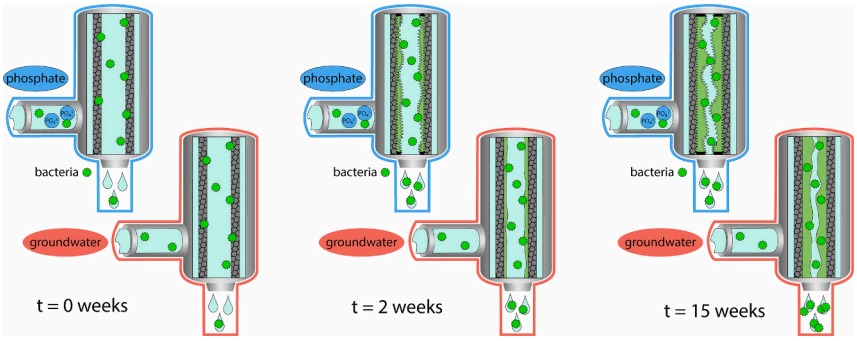

ARTICLE INFO

Editor: Kyle Bibby

Keywords:
Point-of-use filter
Biofilm
Bacteria
Phosphate
Drinking water

ABSTRACT

Point-of-use (POU) filters certified to remove lead are often composed of activated carbon and have been shown to release high concentrations of bacteria, including opportunistic pathogens. In this study, we examine the impacts of the common corrosion inhibitor phosphate on biofilm characteristics and the relationship between biofilm structure and bacterial release from POU filters. This knowledge is essential for understanding how best to use the filters and where these filters fit in a system where other lead contamination prevention measures may be in place. We measured the bacterial release from activated carbon POU filters fed with groundwater - a common source of drinking water - with and without phosphate. We used optical coherence tomography (OCT) to quantitatively characterize biofilm growing on activated carbon filter material in which the biofilms were fed groundwater with and without phosphate. Phosphate filters released significantly less (57–87 %) bacteria than groundwater filters, and phosphate biofilms (median thickness: 82–331 μm) grew to be significantly thicker than groundwater biofilms (median thickness: 122–221 μm). The phosphate biofilm roughness ranged from 97 to 142

* Corresponding author.
E-mail address: gemmagc2@illinois.edu (G.G. Clark).

https://doi.org/10.1016/j.scitotenv.2024.169932
Received 28 August 2023; Received in revised form 29 November 2023; Accepted 3 January 2024
Available online 8 January 2024

% of the groundwater biofilm roughness and was significantly greater in most weeks. Phosphate biofilms also had fewer pores per biofilm volume and shorter channels connecting those pores.

1. Introduction

As drinking water infrastructure continues to age and degrade, commercially available point-of-use (POU) filters, such as those made by Brita and PUR, have become increasingly popular as a temporary solution to address drinking water quality problems. Major concerns about lead and other drinking water contaminants have contributed to 77 % of Americans filtering their drinking water at home (Carollo, 2022). POU filters certified to remove lead are often composed of activated carbon and have been shown to increase bacteria in drinking water (Chaidez and Gerba, 2004; Clark et al., 2022; Nriagu et al., 2018; Tobin et al., 1981; Wu et al., 2017). While not all bacteria are harmful, previous studies have shown that opportunistic pathogens can break through POU filters (Geldreich et al., 1985; Molloy et al., 2007; Wu et al., 2021). In places where lead is a concern, corrosion inhibitors such as orthophosphates and polyphosphates are often applied to control the release of lead into drinking water (McNeill and Edwards, 2002). It is important to understand how the usage of POU filters will pair with other lead contamination prevention measures concerning microbiological drinking water quality.

Biofilms are collections of microorganisms that accumulate and grow on almost any surface (Flemming, 2011; Wingender and Flemming, 2011) and are known to harbor and protect opportunistic pathogens (Cargill et al., 1992; Cooper and Hanlon, 2010; Falkinham, 2015; Wingender and Flemming, 2011). Previous studies have shown that increasing phosphorus concentrations can increase the growth of bacteria and biofilms (Chu et al., 2005; Fang et al., 2009; Hozalski et al., 2005; Noh et al., 2020). Extracellular polymeric substances (EPS) are important for biofilm adhesion (Flemming and Wingender, 2010), and research has shown that adding phosphorus can decrease the production of EPS (Douterelo et al., 2020; Fang et al., 2009; Noh et al., 2020). This may have concerning implications for the combination of using POU filters (which can exacerbate bacteria concentrations in drinking water) and adding phosphate corrosion inhibitors (which may increase bacterial growth and decrease bacterial adhesion to a filter).

Numerous studies have examined biofilm growth on activated carbon as biological activated carbon can be intentionally used in centralized drinking water treatment systems to remove organics (Gibert et al., 2013; Korotta-Gamage and Sathasivan, 2017; LeChevallier et al., 1992; Stringfellow et al., 1993; Urfer et al., 1997; Weber et al., 1978). Biological activated carbon has also been shown to release bacteria (Servais et al., 1994; Stringfellow et al., 1993; Zhang et al., 2015), especially when filtration velocity increases as high shear forces can slough bacteria off of a biofilm (Abe et al., 2012; Paul et al., 2012; Zhang et al., 2015). However, no research has yet examined the characteristics of biofilms growing on POU filters. Biofilm characteristics, such as biofilm thickness, roughness, and pore structure, can influence bacterial adhesion and detachment, biofilm growth, and nutrient transport within the biofilm (Ammar et al., 2015; Carrel et al., 2018; Huang et al., 2020; Huang et al., 2023; Nerenberg, 2016; Picioreanu et al., 2000; Shen et al., 2015; Stewart, 2003; Wu et al., 2012). Understanding the factors governing bacterial release and biofilm growth on activated carbon is key to controlling bacterial release from these popular filters and protecting public health.

To fill this gap in research and understand how phosphorus may affect biofilm characteristics and bacterial release from filters, we have characterized the surface structure and the spatial pore structure of biofilm grown on POU filters using optical coherence tomography (OCT) and compared these results to bacterial release from POU filters over time. Experiments were performed using groundwater – a common drinking water source – with and without phosphate, which has previously been shown to affect the structure of biofilm grown on polyvinyl chloride (PVC) (Huang et al., 2023). Our results show how phosphate affects biofilm characteristics of activated carbon biofilm and how these differences affect the release of bacteria from activated carbon POU filters.

2. Material and methods

2.1. Measuring bacteria release from water bottle filters

We measured the concentrations of bacteria entering and exiting Brita water bottle filters (Brita Model BB10) composed of porous solid block activated carbon (Fig. S1a-b), much like those used in larger faucet filters by Brita and other POU filter companies. The total volume of the filter and water bottle cartridge was 750 mL as determined by a tracer test. The filter itself was a smaller cylinder (17.5 mm outer diameter, 8 mm inner diameter, 80 mm long) and housed in a hollow plastic straw within the water bottle. The flow in the water bottle filters was radial from the outside of the activated carbon cylinder to the inside, where filtered water exited through the straw. Sixteen water bottle filters were assembled with controllable influent: eight replicates were fed with groundwater (groundwater filters), another eight with groundwater containing 2 mg/L as PO_4 of phosphate (phosphate filters) to simulate the use of a phosphate corrosion inhibitor (McNeill and Edwards, 2002). The groundwater without disinfectant treatment came from a well beneath Newmark Civil Engineering Laboratory (Urbana, IL) after being passed through a greensand filter to remove iron precipitates. The groundwater's pH ranged from 7.4 to 7.7, alkalinity was typically around 280 mg/L as $CaCO_3$, and the water temperature ranged from 12 to 15 °C, which is within the range of typical household cold water (Bors et al., 2017). Additional water chemistry parameters for this groundwater, including total organic carbon averaging 1–2 mg/L as C, have been reported in previous studies (Clark et al., 2022; Shen et al., 2017). Sodium phosphate dibasic (Sigma-Aldrich) was mixed with groundwater at a final concentration of 2 mg/L as PO_4 for the phosphate filters.

The water bottle filters were operated at room temperature (20–23 °C), which falls within typical household heating and cooling temperatures of 19–24 °C (Booten et al., 2017). A peristaltic pump was used to pump fresh groundwater, or groundwater with 2 mg/L as PO_4 of phosphate, through the filters at a flow rate of 6.5 mL/s for 2 min 3–5 times per week. The flow rate corresponded to a Reynolds number of 1200 for water that flows over the inner surface of the activated carbon cylinder (Text S1). This value is within the range of Reynolds numbers calculated from filter flow rates observed in the field (Clark et al., 2022). At the beginning of each week, 100-mL samples of water entering and exiting each filter were collected before the two-minute filter flushing. The filter flushing acted to displace any stagnant water, introduce new nutrients and bacteria from the groundwater, and simulate infrequent but consistent filter usage with long stagnation periods that one might observe in an office drinking fountain or break room sink.

Aliquots of 700 μL from the 100-mL samples were taken to measure the total cell counts (TCC) and intact cell counts (ICC) from each sample via flow cytometry (Sysmex Partec). TCC were measured by staining the samples with 1X SYBR Green (Invitrogen), and ICC were measured by staining samples with 1X SYBR Green and 30 μM propidium iodide (Invitrogen) (Berney et al., 2008; Hammes et al., 2008). Samples were incubated in the dark at 37 °C for 10 min between staining and measurement (Van Nevel et al., 2013). Concentrations of bacteria were quantified using the flow cytometer's volumetric counting and the FloMax (Sysmex) software's electronic gating (Hammes et al., 2008). QA/QC calibration beads (Sysmex) were used to check the alignment of

the instrument's lasers and the consistency of the instrument settings. Before sample measurements, the flow cytometer was cleaned with 10 % bleach, nanopure water, and Sysmex Cleaning Solution. Nanopure water was used as a negative control and also used to rinse the instrument in between samples. The limit of quantification was 20 cell counts/mL and the limit of detection was 5 cell counts/mL.

Every two weeks, each of the remaining volumes of the 100-mL samples after flow cytometry processing were filtered through a 0.2-μm cellulose nitrate filter (mdi Membrane Technologies). We used a FastDNA SPIN Kit for Soil (MP Biomedicals) to extract DNA from the filter's surface and performed qPCR on the DNA extract targeting the 16S rRNA universal bacteria gene (Table S1, Text S2) to complement the flow cytometry results. Primers and standard sequences were taken from Shen et al., 2017. Every qPCR plate contained a standard curve made from triplicate serial dilutions of the 16S gene standard and triplicate negative controls. Triplicates of each sample were measured. Each reaction well contained 15 μL of solution containing 2 μL of the sample, standard, or negative control; 4.3 μL of molecular grade water, 0.6 μL of 10 μM forward primer, 0.6 μL of 10 μM reverse primer, and 7.5 μL of 2X PowerUp SYBR Green (Applied Biosystems). The limit of quantification was 5 gene copies (gc) per mL sample, and bacteria were not detected in any of the negative controls. The qPCR efficiency ranged from 92 % to 97 % ($R^2 = 0.989–0.999$).

2.2. Growing biofilm in reactors to acquire biofilm characteristics

In parallel with the water bottle setup, CDC biofilm reactors (Bio-Surface Technologies) were used to grow biofilm on slices of the activated carbon water bottle filters. The biofilm reactors with sliced filter material were used so that the biofilm could be characterized at regular time intervals without sacrificing the entire filter and so that the filter apparatus would not have to be deconstructed - and therefore the biofilm disturbed - in preparation for the characterization methods. Water bottle filters (identical to those used in the water bottle setup in Section 2.1) were cut into 3–5 mm thick slices and glued to polycarbonate coupons that were inserted into polypropylene rods (Fig. S1c). The reactors were autoclaved, and then the activated carbon slices were submerged in groundwater or groundwater containing 2 mg/L as PO_4 of phosphate. Autoclaving the activated carbon filters may have opened more pores in the filter, as steam does during the activation of producing activated carbon. Although the polymers holding the activated carbon block together may have been heat sensitive, the filter did not break or change in any form detected by optical coherence tomography (OCT). Fresh groundwater with or without phosphate was pumped into the reactors from 10 L tanks that were replenished with fresh influent every 2–3 days. The reactors contained a 45 mm agitator that was set to 40 rpm, which corresponds to a Reynolds number of 1200 for water flowing over the surface of the activated carbon slices (Text S1). The matching Reynolds number in the biofilm reactors and the water bottle filters was used to standardize the approximate flow that would pass over the biofilm surface. These reactors were wrapped in aluminum foil to limit algal growth and photosensitive reactions and operated at room temperature (20–23 °C).

Optical coherence tomography (OCT) is a noninvasive imaging technique that has previously been used to characterize biofilm structure and development (Huang et al., 2020; Huang et al., 2023; Janjaroen et al., 2013; Nguyen et al., 2013; Nguyen et al., 2010; Shen et al., 2016; Shen et al., 2015; Xi et al., 2006). At various time intervals (2, 4, 5, 6, 7, 8, 11, and 15 weeks), a slice of activated carbon was removed from each reactor fed with groundwater or groundwater with phosphate. Each week that slices were removed from the reactors, three sets of 100 cross-sectional images of the biofilm were taken using OCT (Fig. S2) for each biofilm type (groundwater biofilms or phosphate biofilms) at different locations to account for the heterogeneity of the biofilm. Using previously described methods (Huang et al., 2020; Huang et al., 2018), OCT images with scanning dimensions 3.13 mm × 4.18 mm × 4 mm were collected.

2.3. Calculating biofilm thickness and roughness from OCT images

A total of 3000 OCT images were analyzed in this study: 1500 from groundwater biofilms and 1500 from phosphate biofilms. The 100 cross-sectional OCT images of each biofilm were preprocessed in ImageJ 2.3 (Fiji) using the following successive steps (Fig. S3):

1) We removed specular artifacts caused by the light from the super-luminescent diode reflecting off water droplets at the biofilm surface.
2) Using the segmented line tool, we marked the interface between the activated carbon surface and the biofilm with pure black (R: 0, G: 0, B: 0) as shown in Fig. S2. Biofilm was differentiated from activated carbon by comparing images of samples with biofilm to control images of fresh activated carbon without biofilm.
3) We used the thresholding function in ImageJ to produce a binary black-and-white image that distinguishes the surface of the biofilm (white) from the air (black) above.

After each successive step, we exported each slice in the image stack to a single file. A MATLAB code (Derlon et al., 2012; Folmli, 2011) for analyzing OCT images of biofilm was translated into Python and updated to process our image stacks (Fig. S3). The updated Python code was verified by processing a subset of images with the MATLAB code and Python code. The difference between the results of the two codes averaged $<10^{-12}$ μm which is well below the resolution of the OCT imaging system.

The new Python code read in all images produced in each of the three successive steps above. Although thresholding was done manually with ImageJ in the third step, an auto-thresholding function was an option in the code. The biofilm interface with the air was detected from the binary image. For each pixel column in the image, the biofilm thickness was calculated by subtracting the marked biofilm-carbon interface from the biofilm-air interface. Finally, the average biofilm thickness (Eq. 1), roughness (Eq. 2), and relative roughness (Eq. 3) were calculated for each image slice using the following equations obtained from previous studies (Derlon et al., 2012; Janjaroen et al., 2013; Picioreanu et al., 1998; Shen et al., 2018):

$$Average\ biofilm\ thickness = \bar{z} = \frac{1}{n}\sum_{i=1}^{n} z_i \tag{1}$$

$$Absolute\ biofilm\ roughness = R_a = \frac{1}{n}\sum_{i=1}^{n} (|z_i - \bar{z}|) \tag{2}$$

$$Relative\ biofilm\ roughness = R_a' = \frac{1}{n}\sum_{i=1}^{n} \left(\frac{|z_i - \bar{z}|}{\bar{z}}\right) \tag{3}$$

where n is the number of pixel columns (thickness measurements counts), z_i is the biofilm thickness for the i^{th} pixel column (μm), and $\bar{z}$ is the mean biofilm thickness (μm).

The biofilm thickness produced by this code was the optical biofilm thickness. To calculate the physical biofilm thickness, we divided by the refractive index 1.3, which was previously determined for biofilms (Huang et al., 2020). Both the absolute and relative biofilm roughness were calculated from the profile of the biofilm's surface and were therefore not affected by the refractive index.

The Python code produced a set of images which were used to verify that the biofilm was correctly identified by the code. This included a set of images marking the location of the biofilm surface (biofilm-air interface), and a set of black-and-white images in which the biofilm was white and everything else was blacked out including the air above and to the sides of the biofilm, and the activated carbon marked below the biofilm. The blackout image set was used when constructing a three-dimensional biofilm model.

2.4. Reconstructing the biofilm

Biofilm reconstruction was performed in Avizo (Thermo Fisher Scientific) by adapting methods developed in previous studies (Carrel et al., 2018; Huang et al., 2020) to fit our biofilm grown on activated carbon. A flow diagram of the biofilm reconstruction methods is shown in Fig. S3. First, we uploaded the raw OCT image stack and the blackout image stack from the Python code to Avizo. Using the thresholding function on the blackout images, we defined the biofilm volume (biomass and pores). We examined each slice in the image stack to correct for any image artifacts produced by the code, and this corrected image made up the biofilm volume. To reduce noise in the raw OCT image stack, we used the Avizo "despeckle" function. From this despeckled image, we defined the pore spaces using the Avizo "top-hat" function every ~20 image slices in the 100-image stack. Pixels with an intensity of zero were considered to be pores. Some of the pixels with an intensity of zero include locations outside of the biofilm such as in the air or the activated carbon. Therefore, we removed these points from the pore space with the Avizo "mask" function using the defined biofilm volume. This yielded the biomass space and the pore space. The defined biomass space and pore space were then used to construct a three-dimensional model of the biofilm. The porosity of the biofilm was calculated from the volume of pore spaces divided by the volume of the biofilm. From the pore space, we analyzed the pore network further by modeling the spatial distribution of pores, represented by spheres, and channels connecting the pores, represented by cylinders.

2.5. Statistical analyses

The data were analyzed using R (version 4.0.4). Independent samples were compared with two-sample *t*-tests if they were normally distributed or the Wilcoxon rank-sum test if either sample was not normally distributed. Dependent samples were compared with paired-sample t-tests if they were normally distributed or Wilcoxon signed-rank tests if they were not. Shapiro-Wilk tests were used to determine the normality of the samples. A significance level of $\alpha = 0.05$ was used for all statistical tests.

3. Results and discussion

3.1. Phosphate-fed filters released less bacteria than groundwater-only filters

The cell counts entering both groundwater and phosphate filters in Week 0 were significantly higher than those exiting ($p < 0.05$), indicating that new filters trap bacteria and thereby remove bacteria from the filtered effluent (Fig. 1). However, in subsequent weeks, effluent bacteria concentrations were significantly higher than influent bacteria concentrations for both the groundwater filters (2.6–6.6 times higher) and the phosphate filters (1.4–4.7 times higher) ($p < 0.05$).

The means, standard deviations, medians, and ranges of the absolute bacteria concentrations released from the groundwater and phosphate filters are shown in Table 1. Absolute bacteria refer to the raw measured bacteria concentrations; normalized bacteria refer to the effluent bacteria divided by the influent bacteria and are shown in Table S2. All samples measured with flow cytometry exceeded the 20 counts/mL limit of quantification. In Weeks 4, 6, 8–11, 13–14, the absolute concentrations of total bacteria released from groundwater filters were significantly greater than those released from phosphate filters ($p < 0.05$) with phosphate filters releasing 57–87 % of the bacteria released by groundwater filters (Table 1). In Weeks 1–3, 5, 7, 12, and 15, there was not a significant difference between the total bacteria released from the groundwater or the phosphate filters ($p > 0.05$). When normalized by the concentration of bacteria entering the filters, the total bacteria released from groundwater filters was greater than that from phosphate filters in Weeks 2, 3, 7, and 12 as well ($p < 0.05$) (Table S2). However, after normalizing by the influent bacteria concentrations, bacteria released from groundwater filters was less than that from phosphate filters in Week 8 ($p < 0.05$) and not significantly different in Week 11 ($p > 0.05$). The trends of the intact bacteria were similar to those of the total bacteria when comparing bacteria released from groundwater and phosphate filters using both the absolute and normalized data (Table 1).

The trends from the qPCR results generally support the findings observed in the flow cytometry data (Table 1) with bacteria released from groundwater filters being greater than that released from

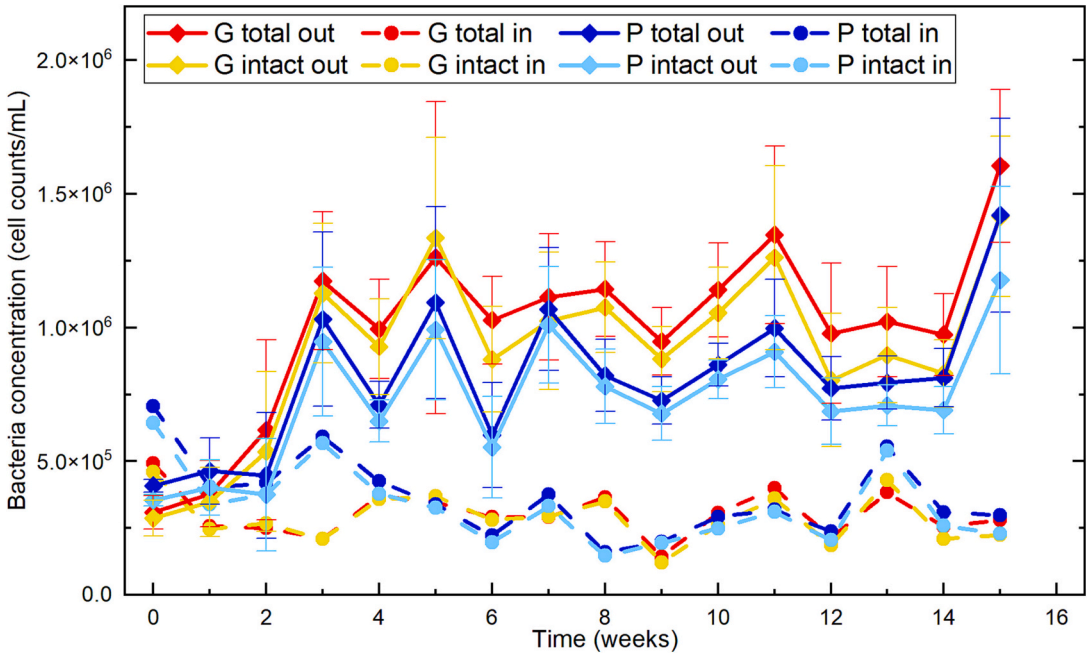

Fig. 1. Time series of average bacteria released (solid lines with square markers) from filters and the bacteria in the feedwater entering the filters (dashed lines with circle markers). Total cell counts are shown in red and blue for the groundwater and phosphate filters, respectively. Intact cell counts are shown in yellow and cyan for the groundwater and phosphate filters, respectively. "G" refers to the groundwater filters and "P" refers to the phosphate filters. Error bars show the standard deviation across 8 filters for each week.

Table 1
Absolute concentrations of bacteria in filter effluent.

Week $\bar{x} \pm s$ med (min-max)	Absolute TCC		Absolute ICC		Absolute 16S	
	groundwater (x10^5 cell counts/mL)	phosphate (x10^5 cell counts/mL)	groundwater (x10^5 cell counts/mL)	phosphate (x10^5 cell counts/mL)	groundwater (x10^2 gene copies/mL)	phosphate (x10^2 gene copies/mL)
0	3.1 ± 0.1 3.1 (2.9-3.3)	4.1 ± 0.2 4.1 (3.7-4.4)	2.9 ± 0.3 2.7 (2.6-3.6)	3.5 ± 0.2 3.5 (3.1-3.8)	6.3 ± 6.9 3.8 (1.4-22.8)	2.0 ± 2.3 1.0 (0.1-6.3)
1	3.8 ± 1.2 3.2 (2.8-6.5)	4.6 ± 1.2 4.8 (2.9-6.8)	3.5 ± 1.3 2.9 (2.5-6.4)	4.0 ± 1.0 4.2 (2.4-5.7)		
2	6.2 ± 3.4 6.0 (2.3-11.0)	4.5 ± 2.4 3.5 (2.0-8.1)	5.4 ± 3.0 5.2 (2.0-10.6)	3.8 ± 2.1 3.0 (1.4-7.2)	88.1 ± 111.3 36.9 (1.7-287.0)	86.5 ± 192.9 22.4 (<LoQ-562.1)
3	11.7 ± 2.6 11.7 (8.3-15.9)	10.3 ± 3.3 9.8 (6.3-17.2)	11.3 ± 2.6 11.3 (7.7-15.2)	9.5 ± 2.8 9.2 (5.7-15.2)		
4	9.9 ± 1.9 9.8 (7.7-12.2)	7.1 ± 0.9 7.2 (5.8-8.5)	9.3 ± 1.8 9.4 (7.1-11.6)	6.5 ± 0.8 6.4 (5.5-7.9)	15.7 ± 26.7 7.8 (0.2-80.8)	11.9 ± 6.3 13.4 (0.8-20.0)
5	12.6 ± 5.8 12.4 (1.0-20.0)	10.9 ± 3.6 9.0 (7.8-16.8)	13.3 ± 3.8 12.0 (10.0-19.2)	9.9 ± 2.6 8.7 (7.4-14.2)		
6	10.3 ± 1.6 9.3 (8.9-12.4)	6.0 ± 2.0 5.3 (3.9-9.3)	8.8 ± 2.0 8.7 (4.7-10.7)	5.5 ± 1.9 4.8 (3.4-8.7)	16.2 ± 17.5 6.7 (1.5-47.4)	699.5 ± 813.6 224.3 (4.2-1785.6)
7	11.1 ± 2.4 10.4 (7.4-15.6)	10.7 ± 2.3 10.7 (8.2-15.0)	10.2 ± 2.6 9.6 (7.0-15.3)	10.1 ± 2.2 9.9 (7.7-14.3)		
8	11.4 ± 1.8 10.9 (9.6-15.4)	8.2 ± 1.4 8.5 (5.9-10.1)	10.8 ± 1.7 10.4 (8.9-14.7)	7.8 ± 1.4 8.0 (5.4-9.9)	39.4 ± 55.6 19.5 (0.3-171.3)	6.5 ± 7.9 2.8 (0.5-20.7)
9	9.5 ± 1.3 9.7 (7.2-10.8)	7.3 ± 0.9 7.0 (6.4-9.1)	8.8 ± 1.2 9.0 (6.9-10.1)	6.8 ± 1.0 6.5 (5.7-9.0)		
10	11.4 ± 1.8 11.3 (9.2-14.4)	8.6 ± 0.8 8.3 (7.6-10.2)	10.5 ± 1.7 10.6 (8.3-13.6)	8.1 ± 0.7 7.9 (7.2-9.5)	6.8 ± 4.8 5.3 (1.1-14.7)	1.7 ± 1.1 1.5 (0.6-3.9)
11	13.5 ± 3.3 12.3 (10.4-20.1)	10.0 ± 1.8 9.8 (7.5-13.2)	12.6 ± 3.4 11.5 (9.2-19.2)	9.1 ± 1.4 8.9 (7.2-10.9)		
12	9.8 ± 2.6 9.0 (6.2-14.8)	7.7 ± 1.2 7.3 (6.5-10.0)	8.0 ± 2.5 7.3 (4.6-12.8)	6.9 ± 1.2 6.6 (5.8-9.4)	10.8 ± 15.2 3.4 (0.3-39.4)	3.0 ± 4.1 1.0 (0.3-11.1)
13	10.2 ± 2.1 10.1 (6.4-13.8)	7.9 ± 1.0 7.9 (6.5-9.4)	9.0 ± 1.8 8.8 (5.8-12.0)	7.1 ± 0.8 6.8 (6.0-8.3)		
14	9.7 ± 1.5 9.8 (6.5-11.5)	8.1 ± 1.1 8.6 (6.1-9.0)	8.3 ± 1.3 8.4 (5.8-9.9)	6.9 ± 0.9 6.8 (5.4-8.0)	3.5 ± 2.9 2.6 (0.5-9.5)	1.1 ± 1.1 0.5 (<LoQ-2.9)
15	16.0 ± 2.9 15.8 (12.2-21.8)	14.2 ± 3.6 13.4 (10.0-20.6)	14.1 ± 3.0 14.0 (8.7-19.0)	11.8 ± 3.5 10.0 (8.8-18.3)		

Rows are highlighted in red on weeks in which the concentration of bacteria was significantly greater in groundwater filter effluent and highlighted in blue on weeks in which phosphate filter effluent was significantly greater. Rows highlighted orange indicate there was no significant difference between the absolute groundwater and phosphate filter effluent bacteria concentrations that week. TCC and ICC stand for total cell counts and intact cell counts, respectively. 16S refers to bacteria measured by qPCR. Values are presented as mean ± standard deviation in the first row of each week and median (minimum-maximum) in the second row of each week. TCC and ICC are in units of 10,000 cell counts/mL and 16S qPCR data are in units of 100 cell counts/mL. <LoQ indicates qPCR samples were below the 5 gc/mL limit of quantification.

phosphate filters in about half of the weeks sampled. All but two samples in Weeks 2 and 14 from the phosphate filter effluent exceeded the 5 gc/mL limit of quantification. The absolute bacteria released from groundwater filters was higher than that from phosphate filters in Weeks 8, 10, and 14 ($p < 0.05$); lower in Week 6 ($p < 0.05$); and not significantly different in Weeks 2, 4, and 12 ($p > 0.05$). After normalizing by the concentration of bacteria entering the filters (Table S2), the concentrations of bacteria exiting groundwater filters were higher than those exiting phosphate filters in Weeks 2, 6, and 12 ($p < 0.05$); lower in Week 8 ($p < 0.05$); and not significantly different in Weeks 4 and 10 ($p > 0.05$). The concentrations of bacteria determined by qPCR were 100–1000 fold lower than those determined by flow cytometry because the DNA extraction process resulted in consistent losses of DNA to remove qPCR inhibitors while the flow cytometry method measured bacteria cells directly.

The rapid elevation of bacterial release with filter age is consistent with previous findings from both the field and laboratory (Clark et al., 2022; Reasoner et al., 1987; Snyder et al., 1995; Su et al., 2009). Numerous studies have reported that phosphate can contribute to increases in microbial growth (Chu et al., 2005; Hozalski et al., 2005; Miettinen et al., 1997); however, the influence of phosphate on microbial activity can actually depend on the environment (Appenzeller et al., 2001; Fang, 2010; Noh et al., 2020). In carbon-limited systems, phosphate addition can have limited impact on bacterial density and biofilm growth (Batté et al., 2003; Noh et al., 2020). The concentrations of carbon and phosphorus in this system were 1–2 mg/L as C and 0.6 mg/L as P (2 mg/L as PO_4), respectively, resulting in a 100:60 to 100:30 carbon to phosphorus ratio. Noh et al., 2020 found a carbon to phosphorus ratio of 100:20 to be an excess phosphorus condition. Although having excess phosphorus could have limited the magnitude by which phosphate increases bacterial growth and release from the filter, the lower release of bacteria from the phosphate filters is likely more attributable to the biofilm structure, which is discussed in Sections 3.2 and 3.3. The results of this study show that filters increase bacteria concentrations after two weeks of usage, but the addition of a phosphate corrosion inhibitor would neither accelerate nor further increase the release of bacteria from POU filters.

3.2. Phosphate biofilms were thicker and rougher than groundwater biofilms

Within two weeks, biofilm had visibly and quantifiably grown on the activated carbon filter media (Fig. 2a, Fig. 3, Fig. S2) to a median thickness of 154 μm in groundwater biofilms and 82 μm in phosphate biofilms (Table S3). Although biofilms were imaged on the outside of the filter, it is reasonable to assume that the biofilm can grow on the inside and outside of the filter because bacteria have been shown to break through the filter (Wu et al., 2021). The median groundwater biofilm thickness ranged from 122 to 221 μm over 15 weeks and the median phosphate biofilm thickness ranged from 82 to 331 μm over the same period (Fig. 2a). In Week 2, the groundwater biofilms were significantly thicker than the phosphate biofilms ($p < 0.05$). Every week thereafter, the phosphate biofilms were significantly thicker than the groundwater biofilms ($p < 0.05$). The periodic rise and fall of the biofilm thickness and the bacterial release were likely due to a combination of natural variation and the filters cycling through stages of filters trapping bacteria and biofilm growth (periods of low bacterial release and thick biofilm) and filters releasing bacteria and biofilm detachment (periods of high bacterial release and thin biofilm).

The absolute roughness of the phosphate biofilms was significantly greater than that of the groundwater biofilms in Weeks 2, 4, 5, 6, and 7 ($p < 0.05$), not significantly different in Weeks 8 and 11 ($p > 0.05$), and significantly lower in Week 15 ($p < 0.05$, Fig. 2b). The mean and median absolute roughness of the phosphate biofilms were 97–142 % and 89 %–145 % that of the groundwater biofilms, respectively. The median absolute roughness ranged from 65 to 79 μm in phosphate biofilms and from 54 to 73 μm in groundwater biofilms (Table S4). When normalizing by the average biofilm thickness to calculate the relative roughness, phosphate biofilms were still significantly rougher than groundwater biofilms in Weeks 2, 4, and 7 ($p < 0.05$, Fig. S4).

Three-dimensional models of the biofilms (Fig. 3a-b) and the pore network (Fig. 3c-d) were developed from the OCT images to further characterize the biofilm. These models provided a visual representation of the biofilm structure and allowed us to quantify the pore structure of the biofilms. Porosity was calculated from the pore volume divided by the total biofilm volume. Biofilm porosity rose and fell over time (Fig. 2c) and ranged from 0.28 to 0.58 in groundwater biofilms (median 0.45) and 0.23–0.58 in phosphate biofilms (median 0.49). There was no significant difference between the porosities of the groundwater and phosphate biofilms in any week ($p > 0.05$). Meanwhile, the total biofilm volume (made up of biomass and pores) of the phosphate biofilms was significantly greater than that of the groundwater biofilms in every week except Week 2 ($p < 0.05$, Fig. 2d, Fig. 3).

Our finding that biofilm thickness and biofilm volume increased with the addition of phosphate aligns with previous studies showing phosphate can increase bacterial activity, biofilm growth, and biofilm thickness (Chu et al., 2005; Fang et al., 2009; Hozalski et al., 2005). This increase in biofilm thickness and volume when phosphate was added was likely due to an increased abundance of phosphorus as a key nutrient for bacterial growth. The addition of phosphate has also been shown to decrease the production of EPS (Douterelo et al., 2020; Fang et al., 2009). EPS has been found to aid biofilm adhesion and bacterial aggregation (Flemming and Wingender, 2010). While decreases in EPS production with the addition of phosphate would indicate that bacteria would be less likely to attach to the fresh activated carbon or biofilm surface, the lower release of bacteria from phosphate filters can be explained by the greater roughness of the phosphate biofilms.

Phosphate biofilms were rougher than groundwater biofilms in most weeks (Fig. 2b, Fig. S4), and phosphate filters released less bacteria than groundwater filters (Fig. 1, Table 2, Fig. S4). Increases in phosphate have been shown to affect species composition in biofilms, favoring microorganisms that can metabolize phosphate (Douterelo et al., 2020; Li et al., 2016). The species composition of a biofilm can be decisive in determining a biofilm's structure, including the biofilm thickness and

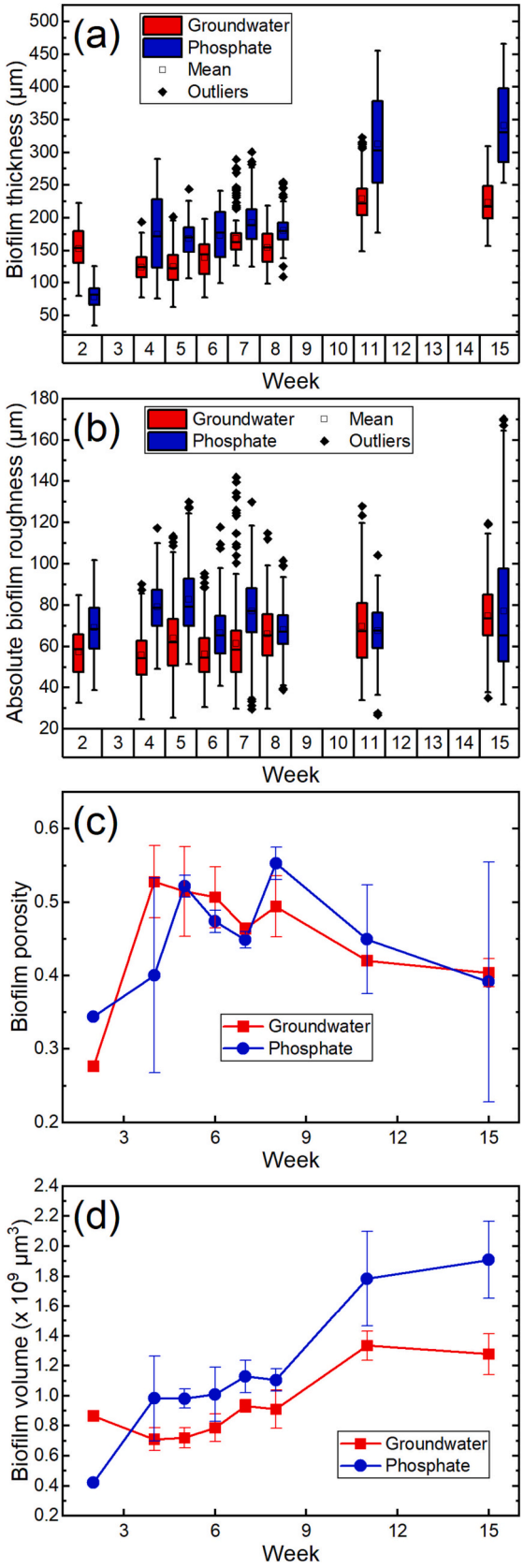

Fig. 2. (a) Biofilm thickness, (b) absolute biofilm roughness, (c) biofilm porosity, and (d) biofilm volume for groundwater and phosphate biofilms after 2, 4, 5, 6, 7, 8, 11, and 15 weeks of biofilm growth in the CDC biofilm reactors.

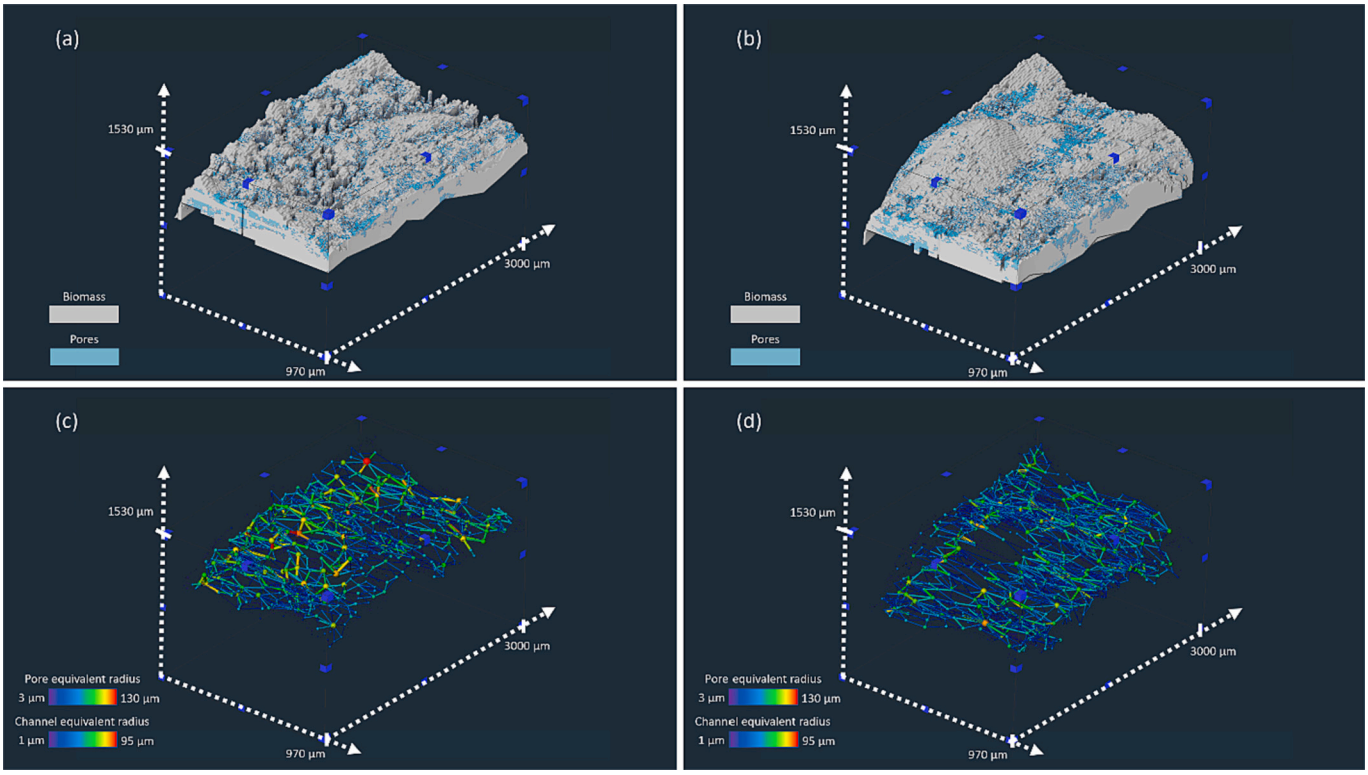

Fig. 3. 3D reconstruction of (a) groundwater biofilms and (b) phosphate biofilms, and the corresponding pore networks for the (c) groundwater biofilm and (d) phosphate biofilm for 15-week old biofilm.

roughness (Murga et al., 1995). The higher roughness of the phosphate biofilms observed in our study may have resulted in less bacterial release from the phosphate filters because of greater bacterial adhesion to and less bacterial detachment from the biofilm.

The relationships observed between higher substrate surface roughness and greater bacterial colonization – including greater adhesion and less detachment – are in agreement with previous studies (Ahmad et al., 2017; Korotta-Gamage and Sathasivan, 2017; Oder et al., 2015; Percival et al., 1999; Shen et al., 2015; Tong and Derek, 2022). The increase in bacterial adhesion to rougher biofilms can be attributable to greater interception of the bacteria by the rough edges of the biofilm and an increased surface area onto which the bacteria could attach (Saranya et al., 2011; Shen et al., 2015; Webster et al., 1999). Rougher biofilms can protect bacteria from detaching by reducing collisions with other particles and reducing the liquid shear (Al-Amshawee et al., 2021; Gjaltema et al., 1997; Shen et al., 2015; Wu et al., 2012). A schematic illustrating this hypothesized influence of roughness on bacterial release is shown in Fig. S5. Our findings suggest that the addition of a phosphate corrosion inhibitor creates a rougher biofilm on the activated carbon POU filter and may help reduce the release of bacteria from the filters.

The overall porosity did not have a clear impact on the bacterial release from filters as there were no consistent differences in the overall porosity between groundwater and phosphate biofilms. After analyzing the pore network of the groundwater and phosphate biofilms, the pore structure of the biofilm could have been influential.

3.3. *Phosphate biofilms had fewer pores and shorter pore-connecting channels than groundwater biofilms*

The axial resolution of the OCT imaging system was 5 µm. OCT can both image structures that are within its imaging resolution (or larger) and detect object structures that are below the optical resolution because of the scattering that comes from sub-resolution structures and results in a "texture" or graininess in the OCT images. This texture in OCT images includes speckle, which is the constructive/destructive interference of coherent light waves scattering off sub-resolution particles or structures within the sample. While we cannot physically resolve or visualize the sub-resolution structures below 5 µm, these structures can still be detected based on the difference in the speckle pattern or texture, as shown in a previous study (Zaki et al., 2023). Given this limitation of the OCT system, pores and channels with equivalent radii below 5 µm were included in the counts of pores and channels but not compared quantitatively.

The number of pores and channels normalized by the biofilm volume for both groundwater and phosphate biofilms were steady over time (Fig. S6). Although the total number of pores were not significantly different in groundwater and phosphate biofilms ($p > 0.05$), groundwater biofilms had significantly more pores normalized by biofilm volume than phosphate biofilms ($p < 0.05$). A distribution of the normalized pore and channel numbers of the groundwater and phosphate biofilms is shown in Fig. 4a. The number of pores per 10^6 µm^3 biofilm ranged from 8.1 to 11.5 (median of 10.5) and 0.2 to 18 (median of 8.7) in groundwater and phosphate biofilms, respectively. The number of channels per 10^6 µm^3 biofilm ranged from 1.0 to 2.4 (median of 1.7) and 0.6 to 4.2 (median of 2.0) in groundwater and phosphate biofilms, respectively.

The distributions of pore equivalent radii, channel equivalent radii, and channel equivalent length are shown in Fig. 4b-d. As shown in the split violin plots with short bodies and long necks, the equivalent radii and lengths were skewed right. Quantitatively, the median equivalent radii and lengths each week (pore equivalent radii: 6–8 µm, channel equivalent radii: 20–26 µm, channel equivalent length: 131–166 µm) were all lower than the mean equivalent radii and lengths in that same week (pore equivalent radii: 10–26 µm, channel equivalent radii: 22–30 µm, channel equivalent length: 148–191 µm).

In Weeks 2, 4, 5, 7, and 15, the channel equivalent length of groundwater biofilms was significantly greater than that in phosphate

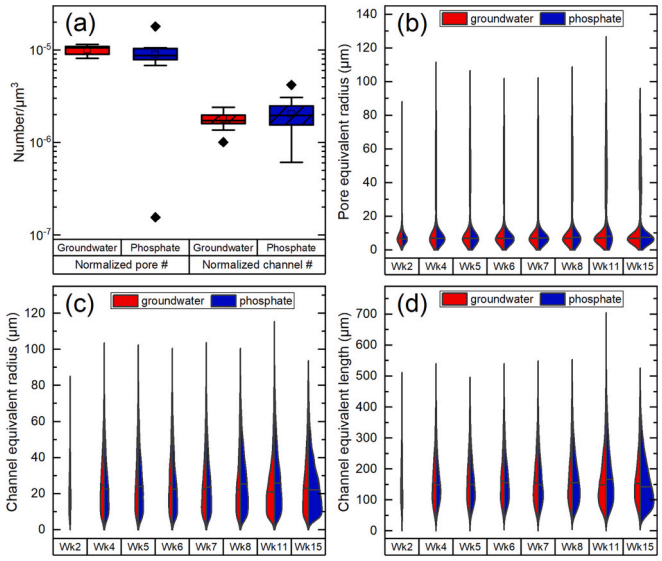

Fig. 4. (a) Boxplots of the number of pores and channels normalized by the total biofilm volume for groundwater and phosphate biofilms. Split violin plots of (b) pore equivalent radius, (c) channel equivalent radius, and (d) channel equivalent length for groundwater and phosphate biofilms. Week is abbreviated "Wk."

biofilms ($p < 0.05$). In other weeks, there was no significant difference between groundwater and phosphate channel lengths ($p > 0.05$). There were some differences in the distributions of pore equivalent radii and channel equivalent radii calculated to be statistically significant when comparing groundwater biofilms against phosphate biofilms. However, the median differences were smaller than the resolution of the OCT imaging system and so the results of those statistical comparisons are not reported. The median pore equivalent radius ranged from 6.7 to 7.0 μm in groundwater biofilms and 6.4–8.0 μm in phosphate biofilms over the 15-week growth period. The median channel equivalent radius ranged from 21 to 25 μm in groundwater biofilms and 20–26 μm in phosphate biofilms. The median channel equivalent length ranged from 149 to 161 μm in groundwater biofilms and 131–166 μm in phosphate biofilms.

In our study, groundwater biofilms had more pores per biofilm volume than phosphate biofilms, and groundwater biofilms had longer channels connecting the pores than phosphate biofilms had. The porosity and pore structure of a material, including biofilms, can affect the stiffness of the material or its ability to resist deformation (Huang et al., 2020; Huang et al., 2023; Laspidou and Aravas, 2007; Savchenko et al., 2014; Schaffler and Burr, 1988). More porous biofilms with longer and larger pore channels can lead to less stiff biofilms (Huang et al., 2020; Huang et al., 2023; Laspidou and Aravas, 2007). Decreases in stiffness can result in more bacteria detaching from the biofilm (Shen et al., 2018; Tierra et al., 2015). This is because the EPS structure becomes more complex with increasing elasticity or decreasing stiffness and forms biofilm streamers that are easier to detach (Tierra et al., 2015). Our findings suggest that the addition of phosphate led to biofilms grown on activated carbon with fewer pores and shorter connecting channels, which may have resulted in a stiffer biofilm less likely to detach bacteria. The structure that a biofilm grows into is likely substrate dependent. Previous studies have shown how bacterial composition dictates biofilm structure (Murga et al., 1995). Our study found that phosphate led to a thicker biofilm with fewer pores and shorter connecting channels when grown on activated carbon. However, a previous study with the same growth conditions found that phosphate led to a thinner and more porous biofilm when grown on PVC (Huang et al., 2023). Our study presents results from Brita activated carbon POU filters. The general structure of commercially available activated carbon POU filters will be similar; however, the impacts of phosphate on the structure of biofilms grown on other filter materials may be different.

4. Conclusions

As POU filters become increasingly popular to remove lead from and improve taste in drinking water, it is essential that we understand the broader impacts of using these filters and how these filters fit in a system with other methods for addressing elevated lead levels in drinking water, such as adding a corrosion inhibitor. Numerous studies have shown that activated carbon POU filters increase concentrations of bacteria in filtered drinking water (Chaidez and Gerba, 2004; Clark et al., 2022; Nriagu et al., 2018; Tobin et al., 1981; Wu et al., 2017), some of which may be opportunistic pathogens (Geldreich et al., 1985; Molloy et al., 2007; Wu et al., 2021). Our study is the first to characterize biofilm grown on activated carbon POU filters and assess the impacts of phosphate on these biofilms. Phosphate filters released significantly less bacteria than groundwater filters in most weeks. Phosphate biofilms were thicker and had a greater surface roughness, which may have resulted in less bacterial release from the phosphate filters. Phosphate biofilms also had fewer pores per biofilm volume and shorter channels connecting the pores, which may have contributed to a less stiff biofilm than the groundwater biofilms, thereby causing less bacterial release from the phosphate filters. In summary, the presence of a phosphate corrosion inhibitor in systems with commercially available activated carbon POU filters could reduce the bacterial release from the filters. This knowledge is important for limiting exposure to and infection from bacteria in drinking water when using POU filters. This study also has broader implications for installing new POU filters in systems where corrosion inhibitors are already in use: that adding a POU filter will not elevate bacteria in drinking water any more than adding a filter would if no corrosion inhibitors were in use.

Declaration of Generative AI in scientific writing

The authors declare that no generative AI or AI-assisted technologies were used in the production of this manuscript, writing or otherwise.

CRediT authorship contribution statement

Gemma G. Clark: Conceptualization, Data curation, Formal analysis, Investigation, Methodology, Visualization, Writing – original draft, Writing – review & editing. **Dietrich Geisler:** Software. **Evan J. Coey:** Data curation, Investigation. **Lance J. Pollitz:** Data curation, Investigation. **Farzana R. Zaki:** Investigation, Resources. **Conghui Huang:** Conceptualization, Methodology. **Stephen A. Boppart:** Resources. **Thanh H. Nguyen:** Conceptualization, Funding acquisition, Supervision.

Declaration of competing interest

The authors declare that they have no known competing financial interests or personal relationships that could have appeared to influence the work reported in this paper.

Data availability

Data will be made available on request.

Acknowledgements

This project was supported by NSF Grant 1855609 and by the NIH/NIBIB Center for Label-free Imaging and Multiscale Biophotonics (CLIMB) Grant P41EB031772. Additionally, the authors would like to thank Amaja Craft, Alexandra Loya, Aarya Patel, and Gang (Hubert) Zheng for their contributions to the laboratory experiments and data analyses.

Appendix A. Supplementary data

Supplementary data to this article can be found online at https://doi.org/10.1016/j.scitotenv.2024.169932.

References

Abe, Y., Skali-Lami, S., Block, J.C., Francius, G., 2012. Cohesiveness and hydrodynamic properties of young drinking water biofilms. Water Res. 46, 1155–1166.

Ahmad, M., Liu, S.T., Mahmood, N., Mahmood, A., Ali, M., Zheng, M.S., et al., 2017. Effects of porous carrier size on biofilm development, microbial distribution and nitrogen removal in microaerobic bioreactors. Bioresour. Technol. 234, 360–369.

Al-Amshawee, S., Yunus, M.Y.B., Lynam, J.G., Lee, W.H., Dai, F., Dakhil, I.H., 2021. Roughness and wettability of biofilm carriers: a systematic review. Environmental Technology & Innovation 21.

Ammar, Y., Swailes, D., Bridgens, B., Chen, J.J., 2015. Influence of surface roughness on the initial formation of biofilm. Surf. Coat. Technol. 284, 410–416.

Appenzeller, B.M.R., Batte, M., Mathieu, L., Block, J.C., Lahoussine, V., Cavard, J., et al., 2001. Effect of adding phosphate to drinking water on bacterial growth in slightly and highly corroded pipes. Water Res. 35, 1100–1105.

Batté, M., Koudjonou, B., Laurent, P., Mathieu, L., Coallier, J., Prévost, M., 2003. Biofilm responses to ageing and to a high phosphate load in a bench-scale drinking water system. Water Res. 37, 1351–1361.

Berney, M., Vital, M., Hülshoff, I., Weilenmann, H.U., Egli, T., Hammes, F., 2008. Rapid, cultivation-independent assessment of microbial viability in drinking water. Water Res. 42, 4010–4018.

Booten, C., Robertson, J., Christensen, D., Heaney, M., Brown, D., Norton, P., et al., 2017. Residential Indoor Temperature Study. U.S. Department of Energy Office of Science and Technical Information.

Bors, J., O'Brien, K.R., Kenway, S.J., Lant, P.A., 2017. Regional-scale variability of cold water temperature: implications for household water-related energy demand. Resour. Conserv. Recycl. 124, 107–115.

Cargill, K.L., Pyle, B.H., Sauer, R.L., Mcfeters, G.A., 1992. Effects of culture conditions and biofilm formation on the iodine susceptibility of Legionella-Pneumophila. Can. J. Microbiol. 38, 423–429.

Carollo, R., 2022. Survey Reveals why More Americans than Ever Are Filtering their Water. Aquasana.

Carrel, M., Morales, V.L., Beltran, M.A., Derlon, N., Kaufmann, R., Morgenroth, E., et al., 2018. Biofilms in 3D porous media: delineating the influence of the pore network geometry, flow and mass transfer on biofilm development. Water Res. 134, 280–291.

Chaidez, C., Gerba, C., 2004. Comparison of the microbiologic quality of point-of-use (POU)-treated water and tap water. Int. J. Environ. Health Res. 14, 253–260.

Chu, C.W., Lu, C.Y., Lee, C.M., 2005. Effects of inorganic nutrients on the regrowth of heterotrophic bacteria in drinking water distribution systems. J. Environ. Manag. 74, 255–263.

Clark, G.G., Pan, W., Giammar, D.E., Nguyen, T.H., 2022. Influence of point-of-use filters and stagnation on water quality at a preschool and under laboratory conditions. Water Res. 211, 118034.

Cooper, I.R., Hanlon, G.W., 2010. Resistance of Legionella pneumophila serotype 1 biofilms to chlorine-based disinfection. J. Hosp. Infect. 74, 152–159.

Derlon, N., Peter-Varbanets, M., Scheidegger, A., Pronk, W., Morgenroth, E., 2012. Predation influences the structure of biofilm developed on ultrafiltration membranes. Water Res. 46, 3323–3333.

Douterelo, I., Dutilh, B.E., Calero, C., Rosales, E., Martin, K., Husband, S., 2020. Impact of phosphate dosing on the microbial ecology of drinking water distribution systems: fieldwork studies in chlorinated networks. Water Res. 187.

Falkinham, J.O., 2015. Common features of opportunistic premise plumbing pathogens. Int. J. Environ. Res. Public Health 12, 4533–4545.

Fang, W., 2010. Biofilm formation and control in a model drinking water distribution system with phosphorus addition. Department of Civil Engineering. Degree of Philosophiae Doctor. National University of Singapore, p. 199.

Fang, W., Hu, J.Y., Ong, S.L., 2009. Influence of phosphorus on biofilm formation in model drinking water distribution systems. J. Appl. Microbiol. 106, 1328–1335.

Flemming, H.C., 2011. Microbial biofouling: unsolved problems, insufficient approaches, and possible solutions. Biofilm Highlights 5, 81–109.

Flemming, H.C., Wingender, J., 2010. The biofilm matrix. Nat. Rev. Microbiol. 8, 623–633.

Folmli, I., 2011. Quantification of Biofilm Morphology Using Optical Coherence Tomography and Quantitative Image Analysis. Master of Science. Swiss Federal Institute of Technology, Zurich.

Geldreich, E.E., Taylor, R.H., Blannon, J.C., Reasoner, D.J., 1985. Bacterial colonization of point-of-use water treatment devices. J. Am. Water Works Assoc. 77, 72–80.

Gibert, O., Lefevre, B., Fernandez, M., Bernat, X., Paraira, M., Calderer, M., et al., 2013. Characterising biofilm development on granular activated carbon used for drinking water production. Water Res. 47, 1101–1110.

Gjaltema, A., van der Marel, N., van Loosdrecht, M.C.M., Heijnen, J.J., 1997. Adhesion and biofilm development on suspended carriers in airlift reactors: hydrodynamic conditions versus surface characteristics. Biotechnol. Bioeng. 55, 880–889.

Hammes, F., Berney, M., Wang, Y., Vital, M., Köster, O., Egli, T., 2008. Flow-cytometric total bacterial cell counts as a descriptive microbiological parameter for drinking water treatment processes. Water Res. 42, 269–277.

Hozalski, R.M., Esbri-Amador, E., Chen, C.F., 2005. Comparison of stannous chloride and phosphate for lead corrosion control. J. Am. Water Works Assoc. 97, 89–103.

Huang, P.C., Chaney, E.J., Shelton, R.L., Boppart, S.A., 2018. Magnetomotive displacement of the tympanic membrane using magnetic nanoparticles: toward enhancement of sound perception. IEEE Trans. Biomed. Eng. 65, 2837–2846.

Huang, C., Sun, P.P., Won, J., Wang, Y., Boppart, S.A., Nguyen, T.H., 2020. Effect of nonphosphorus corrosion inhibitors on biofilm pore structure and mechanical properties. Environ. Sci. Technol. 54, 14716–14724.

Huang, C.H., Clark, G.G., Zaki, F.R., Won, J., Ning, R.S., Boppart, S.A., et al., 2023. Effects of phosphate and silicate on stiffness and viscoelasticity of mature biofilms developed with simulated drinking water. Biofouling 39, 36–46.

Janjaroen, D., Ling, F.Q., Ling, F., Monroy, G., Derlon, N., Morgenroth, E., et al., 2013. Roles of ionic strength and biofilm roughness on adhesion kinetics of Escherichia coli onto groundwater biofilm grown on PVC surfaces. Water Res. 47, 2531–2542.

Korotta-Gamage, S.M., Sathasivan, A., 2017. A review: potential and challenges of biologically activated carbon to remove natural organic matter in drinking water purification process. Chemosphere 167, 120–138.

Laspidou, C., Aravas, N., 2007. Variation in the mechanical properties of a porous multi-phase biofilm under compression due to void closure. Water Sci. Technol. 55, 447–453.

LeChevallier, M.W., Becker, W.C., Schorr, P., Lee, R.G., 1992. Evaluating the performance of biologically-active rapid filters. J. Am. Water Works Assoc. 84, 136–146.

Li, S.S., Wang, C., Qin, H.J., Li, Y.X., Zheng, J.L., Peng, C.R., et al., 2016. Influence of phosphorus availability on the community structure and physiology of cultured biofilms. J. Environ. Sci. 42, 19–31.

McNeill, L.S., Edwards, M., 2002. Phosphate inhibitor use at US utilities. J. Am. Water Works Assoc. 94, 57–63.

Miettinen, I.T., Vartiainen, T., Martikainen, P.J., 1997. Phosphorus and bacterial growth in drinking water. Appl. Environ. Microbiol. 63, 3242–3245.

Molloy, S.L., Ives, R., Hoyt, A., Taylor, R., Rose, J.B., 2007. The use of copper and silver in carbon point-of-use filters for the suppression of Legionella throughput in domestic water systems. J. Appl. Microbiol. 104, 998–1007.

Murga, R., Stewart, P.S., Daly, D., 1995. Quantitative-analysis of biofilm thickness variability. Biotechnol. Bioeng. 45, 503–510.

Nerenberg, R., 2016. The membrane-biofilm reactor (MBfR) as a counter-diffusional biofilm process. Curr. Opin. Biotechnol. 38, 131–136.

Nguyen, C.T., Tu, H.H., Chaney, E.J., Stewart, C.N., Boppart, S.A., 2010. Non-invasive optical interferometry for the assessment of biofilm growth in the middle ear. Biomed. Opt. Express 1, 1104–1116.

Nguyen, C.T., Robinson, S.R., Jung, W., Novak, M.A., Boppart, S.A., Allen, J.B., 2013. Investigation of bacterial biofilm in the human middle ear using optical coherence tomography and acoustic measurements. Hear. Res. 301, 193–200.

Noh, J.H., Yoo, S.H., Son, H., Fish, K.E., Douterelo, I., Maeng, S.K., 2020. Effects of phosphate and hydrogen peroxide on the performance of a biological activated carbon filter for enhanced biofiltration. J. Hazard. Mater. 388.

Nriagu, J., Xi, C., Siddique, A., Vincent, A., Shomar, B., 2018. Influence of household water filters on Bacteria growth and trace metals in tap water of Doha, Qatar. Sci. Rep. 8, 8268.

Oder, M., Kompare, B., Bohinc, K., Torkar, K.G., 2015. The impact of material surface roughness and temperature on the adhesion of Legionella pneumophila to contact surfaces. Int. J. Environ. Health Res. 25, 469–479.

Paul, E., Ochoa, J.C., Pechaud, Y., Liu, Y., Line, A., 2012. Effect of shear stress and growth conditions on detachment and physical properties of biofilms. Water Res. 46, 5499–5508.

Percival, S.L., Knapp, J.S., Wales, D.S., Edyvean, R.G.J., 1999. The effect of turbulent flow and surface roughness on biofilm formation in drinking water. J. Ind. Microbiol. Biotechnol. 22, 152–159.

Picioreanu, C., van Loosdrecht, M.C.M., Heijnen, J.J., 1998. Mathematical modeling of biofilm structure with a hybrid differential-discrete cellular automaton approach. Biotechnol. Bioeng. 58, 101–116.

Picioreanu, C., van Loosdrecht, M.C., Heijnen, J.J., 2000. A theoretical study on the effect of surface roughness on mass transport and transformation in biofilms. Biotechnol. Bioeng. 68, 355–369.

Reasoner, D.J., Blannon, J.C., Geldreich, Edwin E., 1987. Microbiological characteristics of third-faucet point-of-use devices. J. Am. Water Works Assoc. 79, 6.

Saranya, N., Saravanan, S., Moorthi, A., Ramyakrishna, B., Selvamurugan, N., 2011. Enhanced osteoblast adhesion on polymeric Nano-scaffolds for bone tissue engineering. J. Biomed. Nanotechnol. 7, 238–244.

Savchenko, N., Sevostyanova, I., Sablina, T., Gomze, L., Kulkov, S., 2014. The influence of porosity on the elasticity and strength of alumina and zirconia ceramics. International Conference on Physical Mesomechanics of Multilevel Systems 2014 (1623), 547–550.

Schaffler, M.B., Burr, D.B., 1988. Stiffness of compact-bone-effects of porosity and density. J. Biomech. 21, 13–16.

Servais, P., Billen, G., Bouillot, P., 1994. Biological colonization of granular activated carbon filters in drinking-water treatment. J. Environ. Eng.-Asce 120, 888–899.

Shen, Y., Monroy, G.L., Derlon, N., Janjaroen, D., Huang, C., Morgenroth, E., et al., 2015. Role of biofilm roughness and hydrodynamic conditions in Legionella pneumophila adhesion to and detachment from simulated drinking water biofilms. Environ. Sci. Technol. 49, 4274–4282.

Shen, Y., Huang, C.H., Monroy, G.L., Janjaroen, D., Derlon, N., Lin, J., et al., 2016. Response of simulated drinking water biofilm mechanical and structural properties to long-term disinfectant exposure. Environ. Sci. Technol. 50, 1779–1787.

Shen, Y., Huang, C., Lin, J., Wu, W., Ashbolt, N.J., Liu, W.T., et al., 2017. Effect of disinfectant exposure on Legionella pneumophila associated with simulated drinking water biofilms: release, inactivation, and infectivity. Environ. Sci. Technol. 51, 2087–2095.

Shen, Y., Huang, P.C., Huang, C.H., Sun, P., Monroy, G.L., Wu, W.J., et al., 2018. Effect of divalent ions and a polyphosphate on composition, structure, and stiffness of simulated drinking water biofilms. Npj Biofilms Microb. 4.
Snyder, J.W., Mains, C.N., Anderson, R.E., Bissonnette, G.K., 1995. Effect of point-of-use, activated carbon filters on the bacteriological quality of rural groundwater supplies. Appl. Environ. Microbiol. 61, 4291–4295.
Stewart, P.S., 2003. Diffusion in biofilms. J. Bacteriol. 185, 1485–1491.
Stringfellow, W.T., Mallon, K., Digiano, F.A., 1993. Enumerating and disinfecting Bacteria associated with particles released from Gac filter-Adsorbers. J. Am. Water Works Assoc. 85, 70–80.
Su, F., Luo, M., Zhang, F., Li, P., Lou, K., Xing, X., 2009. Performance of microbiological control by a point-of-use filter system for drinking water purification. J. Environ. Sci. (China) 21, 1237–1246.
Tierra, G., Pavissich, J.P., Nerenberg, R., Xu, Z.L., Alber, M.S., 2015. Multicomponent model of deformation and detachment of a biofilm under fluid flow. J. R. Soc. Interface 12.
Tobin, R.S., Smith, D.K., Lindsay, J.A., 1981. Effects of activated carbon and bacteriostatic filters on microbiological quality of drinking water. Appl. Environ. Microbiol. 41, 646–651.
Tong, C.Y., Derek, C.J.C., 2022. Membrane surface roughness promotes rapid initial cell adhesion and long term microalgal biofilm stability. Environ. Res. 206.
Urfer, D., Huck, P.M., Booth, S.D.J., Coffey, B.M., 1997. Biological filtration for BOM and particle removal: a critical review. J. Am. Water Works Assoc. 89, 83–98.
Van Nevel, S., Koetzsch, S., Weilenmann, H.-U., Boon, N., Hammes, F., 2013. Routine bacterial analysis with automated flow cytometry. J. Microbiol. Methods 94, 73–76.
Weber, W.J., Pirbazari, M., Melson, G.L., 1978. Biological growth on activated carbon-investigation by scanning Electron-microscopy. Environ. Sci. Technol. 12, 817–819.
Webster, T.J., Siegel, R.W., Bizios, R., 1999. Osteoblast adhesion on nanophase ceramics. Biomaterials 20, 1221–1227.
Wingender, J., Flemming, H.-C., 2011. Biofilms in drinking water and their role as reservoir for pathogens. Int. J. Hyg. Environ. Health 214, 417–423.
Wu, M.Y., Sendamangalam, V., Xue, Z., Seo, Y., 2012. The influence of biofilm structure and total interaction energy on retention by biofilm. Biofouling 28, 1119–1128.
Wu, C.-C., Ghosh, S., Martin, K.J., Pinto, A.J., Denef, V.J., Olson, T.M., et al., 2017. The microbial colonization of activated carbon block point-of-use (PoU) filters with and without chlorinated phenol disinfection by-products. Environ. Sci. Water Res. Technol. 3, 830–843.
Wu, C.-C., Love, N.G., Olson, T.M., 2021. Bacterial transmission and colonization in activated carbon block (ACB) point-of-use (PoU) filters. Environ. Sci.: Water Res. Technol. 7, 1114–1124.
Xi, C.W., Marks, D., Schlachter, S., Luo, W., Boppart, S.A., 2006. High-resolution three-dimensional imaging of biofilm development using optical coherence tomography. J. Biomed. Opt. 11.
Zaki, F.R., Monroy, G.L., Shi, J., Sudhir, K., Boppart, S.A., 2023. Texture-based speciation of otitis media-related bacterial biofilms from optical coherence tomography images using supervised classification. Res. Square (under review).
Zhang, Y.J., Li, P.F., Zhou, L.L., 2015. Study on the release of HPC and particles in ozonation and biological activated carbon processes. Chem. Eng. J. 276, 37–43.